Tight-binding molecular dynamics study of palladium

A. Shabaev and D. A. Papaconstantopoulos
George Mason University, Fairfax, Virginia 22030, USA
(Received 24 September 2008; published 18 February 2009)

We present a study of palladium by the NRL tight-binding (TB) method. We constructed a set of TB parameters by fitting to first-principles data for the electronic energies of face-centered cubic (fcc) and body-centered cubic (bcc) Pd as a function of volume. This TB Hamiltonian was then used to calculate phonon frequencies and elastic constants. Our calculations show good agreement with experiments and demonstrate the efficiency of the NRL-TB scheme. In addition, we performed tight-binding molecular dynamics simulations to calculate the density of states, coefficient of thermal expansion, mean-squared displacement, and energy of vacancies formation at finite temperature.

DOI: 10.1103/PhysRevB.79.064107 PACS number(s): 71.15.Nc, 71.15.Pd

I. INTRODUCTION

First proposed four decades ago in a seminal paper by Slater and Koster,[1] the tight-binding (TB) method has proven to be a very powerful approach for calculating the total energy, electronic energy bands, and electronic densities of states for a large number of various solid-state structures.[2] The TB method very efficiently and accurately reproduces first-principles data for the electronic band structure and density of states (DOS).[3] Recently the NRL-TB method has been developed to provide transferability between different structures.[2] In this method the parameters of the Slater-Koster Hamiltonian are fit to reproduce a first-principles database of not only the band structures but also the total energies for several crystal structures differing in volume or symmetry.[4,5] The NRL-TB method has been advanced to perform molecular dynamics (MD) simulations.[6] Tight-binding molecular dynamic capabilities have opened possibilities for calculations at finite temperatures by relaxing the positions and determining velocities together with forces on moving atoms in a large supercell.

In this paper we present the results of TB calculations for palladium with a static atomic distribution and with molecular dynamic simulations of atomic motion for a wide range of temperatures, from 0 to 900 K. We apply static and dynamic methods to calculate the structural and electronic properties of bulk palladium and total energy of clusters of various sizes. We find a variety of electronic and structural properties including electron energies, elastic constants, phonon frequencies, vacancy formation energies, and mean-squared displacements.

II. STATIC CALCULATIONS

A. NRL-TB method

The NRL-TB method is based on fitting the onsite terms, the two-center Hamiltonian, and the overlap parameters to the electronic eigenvalues and total energies provided by first-principles calculations. For atom i, the on-site TB parameters are defined as

$$h_{il} = a_l + b_l\rho_i^{2/3} + c_l\rho_i^{4/3} + d_l\rho_i^2, \tag{1}$$

where coefficients a_l, b_l, c_l, and d_l ($l=s$, p, or d) are the fitting parameters and the atom density ρ_i has the form:

$$\rho_i = \sum_j \exp(-\lambda^2 R_{ij}) F(R_{ij}), \tag{2}$$

where the sum is over all atoms j within a range R_c of atom i, λ is a fitting parameter, and $F(R_{ij})$ is a cutoff function. In the two-center approximation, the hopping integrals depend only on the angular momentum dependence of the orbitals, $ll'u$ ($ss\sigma$, $sp\sigma$, $pp\sigma$, $pp\pi$, $sd\sigma$, $pd\sigma$, $sd\pi$, $dd\sigma$, $dd\pi$, and $dd\delta$) and the distance between the atoms. The hopping parameters for both the Hamiltonian and overlap matrices have the form

$$H_{ll'u}(R) = (e_{ll'u} + f_{ll'u}R + g_{ll'u}R^2)\exp(-q_{ll'u}^2 R)F(R), \tag{3}$$

where R is the separation between the atoms and $(e_{ll'u}, f_{ll'u}, g_{ll'u}, q_{ll'u})$ are the fitting parameters. This form of the TB parameters allows transferability to different crystal structures and atomic configurations.

We first find the set of the TB parameters by fitting the electronic energies for a static distribution of atoms located at fixed lattice coordinates. For a monatomic system with the s, p, and d orbitals included into a basis, the NRL-TB parametrization method requires 93 parameters to reproduce the electronic band structure and the total energy available from the first-principles calculations in a wide range of lattice constants for various lattice structures.[2] We have found the set of TB parameters fitting the linearized augmented planewave (LAPW) calculations for the bcc using 55 k points and the fcc using 89 k points in the irreducible Brillouin zone. The latter has a minimum of the total energy at lattice constant $a=3.847$ Å that corresponds to $v_c=a^3/4 = 14.24$ Å^3 of the volume of the primitive cell. The lattice constant is fit to the LAPW value of 3.85 Å, which underestimates by 1% the experimental value of 3.89 Å. The resulting nonorthogonal set of parameters obtained from the fit predicts the electronic band structure and the total energy for simple cubic (sc) and hexagonal close-packed (hcp) structures which were not fitted. Figure 1 shows total energy plotted as a function of the primitive cell volume for the fcc, bcc, sc, and hcp structures. Each structure has its own minimum of the total energy. The minimum of the fcc structure, as expected, is the lowest one followed by the hcp, bcc, and sc structures. The sc structure has the highest energy at the minimum. The hcp structure is shown for the c/a ratio of

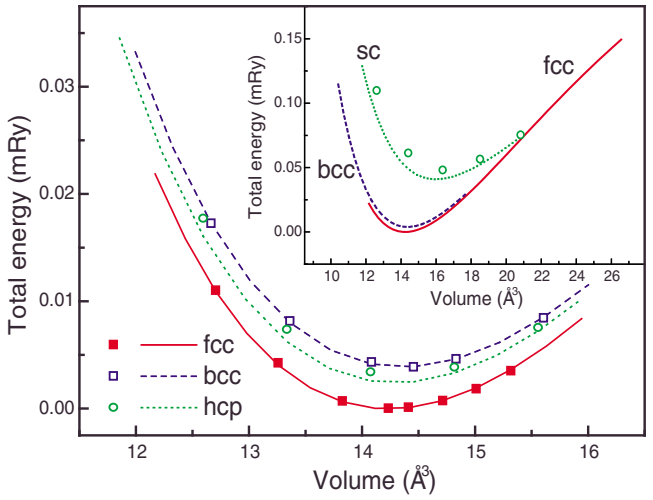

FIG. 1. (Color online) Total energy of various palladium structures: lines show TB results for fcc (solid red), bcc (dashed blue), and hcp(dotted green) with $c/a=1.72$; symbols show LAPW data for fcc (closed squares), bcc (open squares), and hcp (open circles). Inset: total energy of fcc, bcc, and sc structures; open circles show LAPW data for sc.

1.72 with the lowest minimum for the hcp structures. The TB calculations are compared with the LAPW results with almost perfect match for the bcc and fcc structures included into fit. Good agreement for the sc and hcp structures demonstrates transferability of the parameters to other structures which were not included into fit. This set of the parameters also works well for the computation of the phonon frequencies and the elastic constants. The same parameters are also used to perform molecular dynamics simulations.

B. Phonon frequencies

Phonon frequencies and elastic constants provide information about the derivatives of the energy with respect to the displacement of the atoms from their equilibrium lattice positions. We have found the phonon frequencies by the frozen phonon method[7] where a unit cell is commensurate with the wave vector of the phonon, and the displacements of atoms are chosen according to the polarization and the phase of the phonon mode. In the harmonic approximation, the phonon frequencies can be determined from the second derivatives of the total energy as a function of the displacement and the energy variation can be written in the form[7]

$$U_{\text{harm}} = \frac{1}{2} \sum_{\mathbf{R},\mathbf{R}',\alpha,\beta} \mathbf{x}^{\alpha}(\mathbf{R})\, \boldsymbol{\eta}^{\alpha\beta}(\mathbf{R}-\mathbf{R}')\mathbf{x}^{\beta}(\mathbf{R}'), \qquad (4)$$

where $\mathbf{x}^{\alpha}$ is the deviation from equilibrium of atom α on unit cell associated with lattice vector $\mathbf{R}$ and $\boldsymbol{\eta}^{\alpha\beta}(\mathbf{R}-\mathbf{R}')$ is the force constant matrix. The higher orders are responsible for anharmonicity[8] which we investigate in the frame of the tight-binding molecular dynamics (TBMD) methods.

Table I shows the phonon frequencies of palladium at several high-symmetry points in the fcc Brillouin zone.[9,10] The calculated frequencies are compared to the experimental values.[11] The overall agreement is very good, with a tendency of larger divergence for longitudinal modes than for the transverse ones; the difference ranges from 0.3% to 18%. It appears that with the exception of the Δ_1 and Σ_2 points, all calculated frequencies are higher than experiment, indicating a systematic shift in the higher frequencies. The shift can be possibly explained by the smaller lattice constant compared to the experimental value of and variation in the phonon frequency with the temperature,[11] indicating that with the current TB parameters the energy variation is slightly stronger with the displacement. We repeated our calculations of the phonon frequencies at the experimental value of the lattice parameter which is 1% higher than the TB equilibrium value. The results did not show significant differences.

C. Elastic constants

The calculation of the elastic constants can serve as a sensitive test for the TB parameters because the calculations depend on small differences between the equilibrium energies and the energy with the strain. The total energy changes by an amount,[12]

TABLE I. Phonon frequencies of palladium (in tetrahertz)

Coordinates	Symmetry	Polarization	NRL-TB	Experiment[11]	% Difference
(0,0,4) $\frac{\pi}{4a}$	Δ_1	Longitudinal	4.19	4.76	12%
	Δ_5	Transverse	3.14	3.13	0.3%
(0,0,8) $\frac{\pi}{4a}$	X_3	Longitudinal	7.42	6.72	10%
	X_5	Transverse	4.68	4.59	2%
(0,4,8) $\frac{\pi}{4a}$	W_2	Longitudinal	4.65	4.19	11%
	W_5	Transverse	6.04	5.55	9%
(4,4,0) $\frac{\pi}{4a}$	Σ_1	Longitudinal	6.21	5.91	5%
	Σ_2	Transverse	2.81	2.88	2%
	Σ_3	Transverse	4.71	4.45	6%
(4,4,4) $\frac{\pi}{4a}$	L_2	Longitudinal	8.06	6.85	18%
	L_3	Transverse	3.33	3.20	4%

TABLE II. Elastic constants for palladium (in GPa).

	NRL-TB	LAPW	Expt.[a]
$\frac{1}{2}(C_{11}-C_{12})$	28.23	29.5[b]	29.00
C_{44}	60.52	65[b]	71.05
B	223.07	224.9	195.05

[a]Reference 13.
[b]Reference 14.

$$E(e_i) = E_0 - P(V)\Delta V + \sum_{i=1}^{6}\sum_{j=1}^{6} C_{ij}e_i e_j/2 + O[e_i^3], \quad (5)$$

where V is the volume of undistorted lattice, $P(V)$ is the pressure, ΔV is the change in the volume of the lattice due to the strain, and e_i are the strain tensor components. In general, there are 21 elastic constants C_{ij}. This number is reduced to three for the cubic lattices (fcc, bc, and sc). Applying the volume-conserving orthorhombic strain,

$$e_1 = -e_2 = \xi,$$

$$e_3 = \xi^2/(1-\xi^2),$$

$$e_4 = e_5 = e_6 = 0, \quad (6)$$

we obtain the tetragonal shear modulus $(C_{11}-C_{12})/2$ from Eq. (5), which can be written as

$$\Delta E(\xi) = \Delta E(-\xi) = V(C_{11}-C_{12})\xi^2 + O[\xi^3]. \quad (7)$$

Similarly, by applying the volume-conserving monoclinic strain,

$$e_6 = \xi \quad e_3 = \xi^2/(4-\xi^2),$$

$$e_1 = e_2 = e_4 = e_5 = 0, \quad (8)$$

we find the trigonal shear modulus C_{44} from Eq. (5) that takes the form

$$\Delta E(\xi) = \Delta E(-\xi) = VC_{44}\xi^2/2 + O[\xi^3]. \quad (9)$$

The third independent elastic constant can be calculated from the relation to the bulk modulus

$$B = (C_{11} + 2C_{12})/3. \quad (10)$$

Using the energy found for various volumes [Fig. 1], we can calculate the bulk modulus near the minimum of the fcc structure as $B = -V \cdot \Delta P/\Delta V$.

Table II shows the results of the TB calculations in comparison with the experimental data[13] and our LAPW results. Following the LAPW with less than 10% deviation, the monoclinic strain and trigonal shear modulus are below the experimental values and the bulk modulus is about 15% larger than the experimental value.

III. ENERGY OF CLUSTERS

To further demonstrate the robustness of our TB Hamiltonian and capabilities of the NRL-TB method we found the energy of Pd clusters consisting of various numbers of atoms arranged in the fcc structure. We calculated energy per one atom for static clusters with sequentially filled shells of neighbors equally distant from the central atom of the cluster, including 13, 19, 43, 55, 79, 141, 177, 225, 381, 555, 767, and 935 atoms. The results are shown in Fig. 2. The energy decreases with size as expected asymptotically approaching to the bulk limit of 0 mRy.

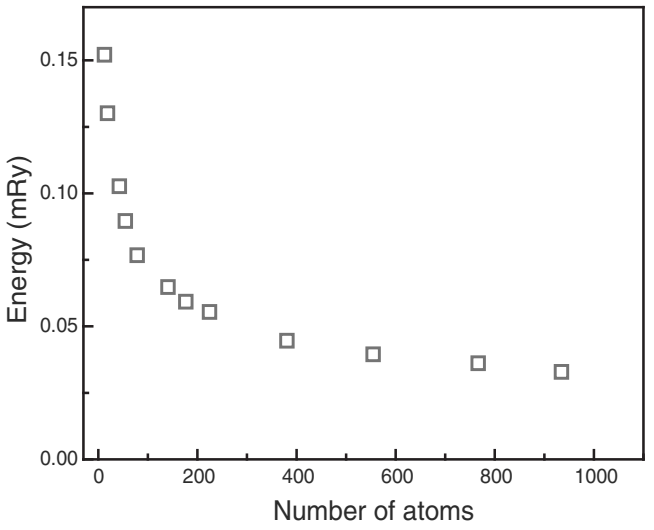

FIG. 2. Total energy per one atom of fcc Pd clusters.

IV. MOLECULAR DYNAMICS SIMULATIONS

Using the NRL-TB parameters we performed the MD simulations for a supercell of Pd containing 64 atoms that is obtained by repeating the primitive cell four times along each of the primitive lattice directions. The simulations were performed for 3000 steps with a time step of 2 fs. Figure 4(a) shows the supercell at the start of the simulation. Initially, the atoms are placed on the fcc lattice with random velocities with a Boltzmann distribution function for a temperature of $2T$. Very quickly (see Fig. 3), in approximately 70 fs (35

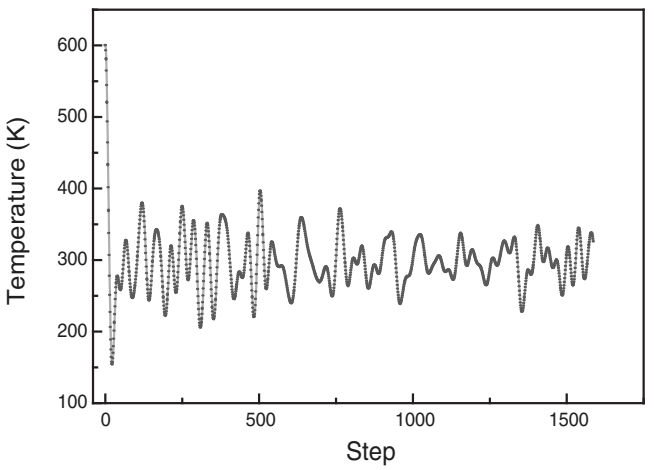

FIG. 3. Change in temperature in MD simulations of 64 palladium atoms with time increment of 2 fs/step.

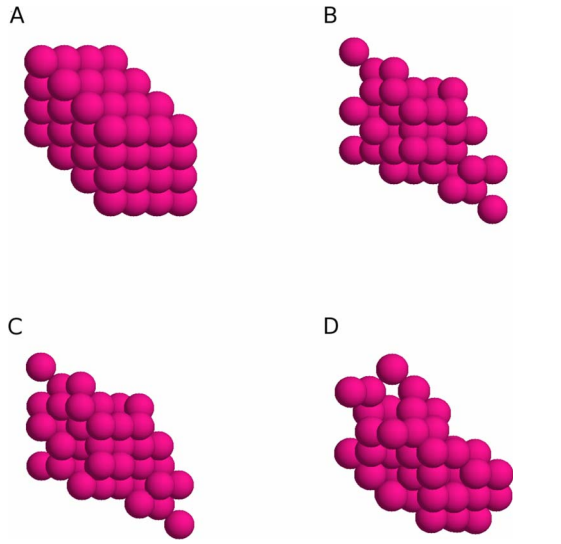

FIG. 4. (Color online) Evolution of palladium supercell consisting of 64 atoms: (A) initial fcc structure at $T=1800$ K; (B) 4 fs elapsed time at $T=1778$ K; (C) 16 fs elapsed time at $T=1392$ K; and (D) 1898 fs elapsed time at $T=955$ K.

steps), the atomic motion slows down [Figs. 4(b) and 4(c)] to the average velocities corresponding to the equilibrium at temperature T. The fluctuations are reduced to the normal equilibrium scale approximately in a picosecond time range [Fig. 4(d)].

A. Coefficient of thermal expansion

We applied the TBMD method to investigate the anharmonicity of the lattice energy. Additional information about the anharmonicity can be deduced from the calculations of the coefficient of thermal expansion and the mean-squared displacement. To evaluate qualitatively the anharmonicity we consider the following simple equation for the change in the energy with the displacement of an atom from its equilibrium position:

$$U(x) = \frac{1}{2}\eta x^2 - \frac{1}{3}\gamma x^3 + \frac{1}{4}\delta x^4, \tag{11}$$

where we included the anharmonic terms up to the fourth order of the displacement, x. The first term is the harmonic part; the second and the third terms are responsible for the thermal expansion coefficient and the mean-squared displacement. The probability of an atom to deviate from its equilibrium can be defined as

$$P(x) = \left(\frac{\eta}{2\pi kT}\right)^{1/2} e^{-U(x)/kT}. \tag{12}$$

Assuming that the anharmonic terms are small, we expand the probability

$$P(x) = \left(\frac{\eta}{2\pi kT}\right)^{1/2}\left[1 + \frac{1}{3kT}\gamma x^3 - \frac{1}{4kT}\delta x^4\right] e^{-\eta x^2/2kT} \tag{13}$$

and find the average displacement as

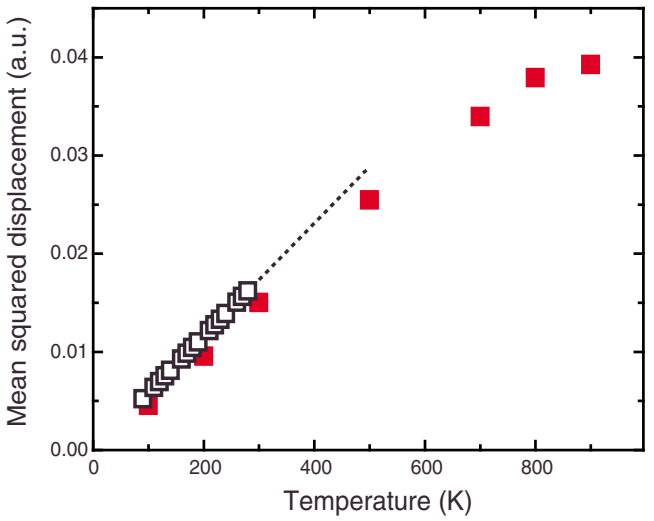

FIG. 5. (Color online) Mean-squared displacement for palladium: calculations (closed squares) and experiment (Ref. 16) (open squares) with linear extrapolation (dashed line).

$$\langle x\rangle = \frac{\gamma}{3kT}\left(\frac{\eta}{2\pi kT}\right)^{1/2}\int_{-\infty}^{\infty} x^4 e^{-\eta x^2/2kT} dx = \frac{\gamma k}{\eta^2}T, \tag{14}$$

where only the second term of odd order is included. The linear coefficient of thermal expansion is the average displacement per unit length and temperature

$$\alpha_L = \frac{\gamma k}{a\eta^2}. \tag{15}$$

The linear coefficient can be found from the TBMD simulations for various temperatures. We first calculate the energy per unit volume or the pressure in the lattice and determine the coefficient from $dP/dT=3\alpha_L B$ where B is the bulk modulus.[6] The pressure changes linearly with the temperature within the entire range of our calculations with the slope of the linear fit 5.52 MPa/K. For the bulk modulus of 180 GPa, we find $\alpha_L=10^{-5}$ K^{-1} that is approximately 10% smaller than the experimental value.[15] This difference is consistent with the higher values of the phonon frequencies and η^2 which are proportional to each other. Using Eq. (15), we estimate the ratio $\gamma k/\eta^2$ as $3.8\cdot 10^{-5}$ Å/K.

B. Mean-squared displacement

We have determined the atomic mean-squared displacement of the Pd atoms for various temperatures using the atomic positions recorded in the process of the MD simulation. In the range of relatively low temperatures, the mean-squared displacement linearly changes with the temperature (Fig. 5). In this range, the results of calculations are in good agreement with the experimental data.[16,17] At higher temperature, the mean-squared displacement is sublinear. This can be explained by an increasing anharmonicity of atomic vibrations at higher temperature.

As with the coefficient of thermal expansion, we similarly find an average of the displacement squared

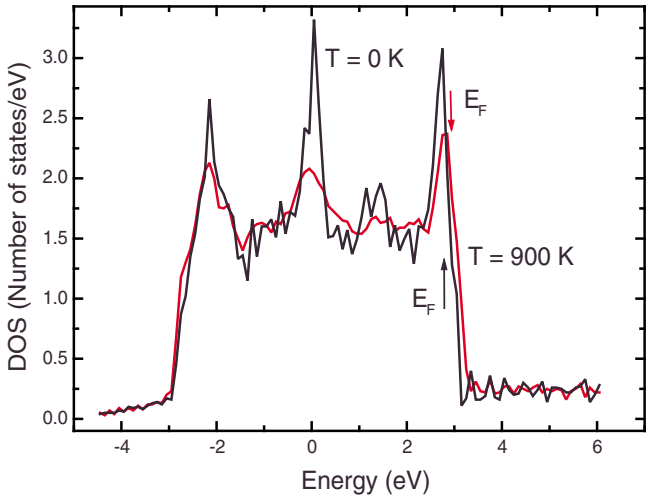

FIG. 6. (Color online) Density of states at two temperatures: 0 and 900 K.

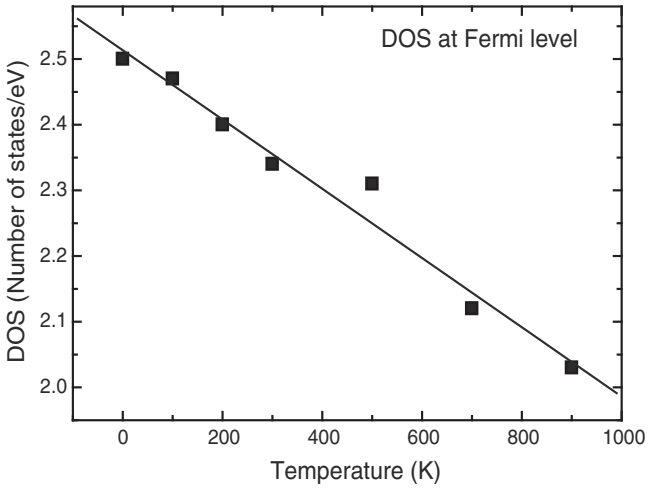

FIG. 7. Density of states at the Fermi level as a function of temperature.

$$\langle x^2\rangle = \left(\frac{\eta}{2\pi kT}\right)^{1/2}\int_{-\infty}^{\infty}\left[x^2 - \frac{1}{4kT}\delta x^6 + \frac{1}{9k^2T^2}\gamma^2 x^8\right]e^{-\eta x^2/2kT}dx$$

$$= \frac{kT}{\eta}\left(1 - \frac{15\delta}{4\eta}\frac{kT}{\eta} + \frac{35\gamma^2}{3\eta^2}\frac{kT}{\eta}\right), \tag{16}$$

where we use only the even orders of the energy expansion in Eq. (11).

At relatively low temperature, the mean-squared displacement is a linear function of temperature with the slope of $k/\eta = 1.87\cdot 10^{-5}$ Å^2/K close to the slope of experimental data. The mean-squared displacement begins deviating from the linear trend at temperatures above the Debye temperature $\Theta_D = 274$ K (Ref. 18) that is consistent with the anharmonic changes of the phonon frequencies.[11] Both the cubic and quartic terms of energy in Eq. (11) give contributions to the anharmonicity of the mean-squared displacement. The coefficient originating from the cubic term is $35\gamma^2/(3\eta^2) = 48$ Å^{-2} that is smaller than its quartic counterpart $15\delta/(4\eta) = 222$ Å^{-2}. We can conclude that the quartic coefficient is apparently excessive since one would expect the anharmonic deviations to become relatively large at higher temperatures approaching to the melting point where the displacement is comparable to the lattice constant.

C. Density of states

We have determined the electronic DOS and the position of the Fermi level for various temperatures in the range of 0–900 K. The density of states is found by counting the number of eigenvalues within a bin of 0.1 eV width over all k points included in the calculations.

At zero temperature the DOS of palladium has a sharp maximum near the Fermi level (Fig. 6) which is approximately the energy where the d bands end. The peaks flatten as the temperature increases. Apparently this sharp change in energy requires a higher number of k points for the molecular dynamic simulations to increase the precision in the calculations of forces. We determined that at least 108 k points were needed for the supercell of 64 atoms to provide stability of the MD simulations. The TBMD method substantially reduces the computational cost in comparison with first-principles methods which currently appear to be not practical for such massive calculations.

Figure 6 shows the DOS of palladium for 0 and 900 K with arrows pointing to the position of the Fermi level varying with the temperature: $E_F(T)$. At zero temperature, the Fermi level is determined by

$$\int_{-\infty}^{E_F(0)} D(E,0)dE = N_e, \tag{17}$$

where $D(E,0)$ is the density of states at zero temperature and N_e is the total number of electrons populating the energy states below the Fermi level. This implies that the population of the electrons is the step function of energy,

$$f(E) = \begin{cases} 1, & E \le E_F(0) \\ 0, & E > E_F(0) \end{cases}. \tag{18}$$

The step function is a special case of the Fermi-Dirac distribution function

$$f(E,T) = (e^{[E-E_F(T)/kT]} + 1)^{-1}, \tag{19}$$

which turns into Eq. (18) at $T=0$. For temperatures above zero, both the density of states and the Fermi energy vary with the temperature, leaving the total number of electrons unchanged. Instead of Eq. (17), the integral for the total number of electrons is

$$\int_{-\infty}^{\infty} D(E,T)f(E,T)dE = N_e. \tag{20}$$

This integral determines the position of the Fermi level as a function of temperature.[19] Normally, if the DOS is a relatively smooth function almost not changing with temperature, the Fermi level moves to a lower position with an increase in temperature. Figure 7 shows that the DOS changes with temperature at the position of the Fermi level. One reason for this is the change in the electronic energy levels and

consequently in the DOS with the vibration of atoms in the lattice which become more pronounced at higher temperatures. In palladium the DOS varies sharply near the Fermi level, and therefore the Fermi level shifts to a higher position with the depopulation of the electronic states at higher temperatures.

D. Vacancy formation energy

We have applied the TBMD simulations via the conjugate gradient method for the calculations of vacancy formation. The TBMD methods make it possible to find an energy of vacancy formation in a relatively large supercell to reduce the interaction between the vacancies. The formation energy of M vacancies in a supercell of N atoms is

$$E_{vf} = E(N-M,M) - \frac{N-M}{N}E(N,0), \tag{21}$$

where $E(N,0)$ is the total energy of the supercell containing all N atoms and $E(N-M,M)$ is the energy of the supercell with $N-M$ atoms and M vacancies. After M atoms are removed from the supercell, the supercell relaxes. The atoms are shifted from their normal lattice positions to form M stable vacancies.

We calculated the formation energies of a single vacancy and a divacancy. To improve the convergence, we increased the number of k points to 864 for the TBMDK simulations of the 64 atoms supercell. We have found that the formation energy of the single vacancy is 1.27 eV. The energy formation of the divacancy strongly depends on the position of the vacancies (see Fig. 8) varying from 2.81 eV for the vacancies at the nearest sites along the body diagonal down to 2.53 eV for the vacancies at the nearest sites on the cube side. The minimum of the divacancy formation energy, 2.53 eV, is slightly lower than the formation energy of two single vacancies 2.54 eV, indicating that two vacancies will likely form the divacancy.

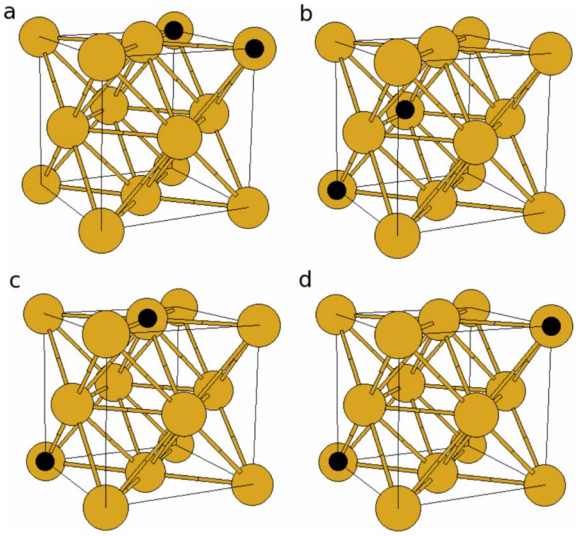

FIG. 8. (Color online) Energy formation of divacancies (positions shown by black dots): (a) 2.52, (b) 2.65, (c) 2.67, and (d) 2.81 eV.

V. CONCLUSIONS

In summary, we have obtained a set of TB parameters for palladium by fitting to LAPW data for the electronic energies of fcc and bcc structures. The resulting TB Hamiltonian was used in static calculations to predict the energy of other structures such as the sc and hcp as well as to calculate elastic constants and phonon frequencies. We also performed MD simulations from which we obtained the vacancy formation energies, mean-squared displacements, coefficient of thermal expansion, and temperature dependence of the density of states. The MD calculations exploited the computational speed of the TB method and made it possible to perform calculation of 64 atoms in the unit cell with 108 k points and for 3000 MD steps. Our runs used parallelization of the MD code for up to 32 nodes on an SGI Altix computer. A typical run took approximately 30 h. We expect that a similar calculation using one of the first-principles codes would be more than a factor of 10 slower.

Various characteristics calculated by TB and TBMD methods show good agreement with experimental data. The deviations from experiments possibly originate from underestimation of the lattice constant by the LAPW and slightly excessive anharmonicity of the TB Hamiltonian.

ACKNOWLEDGMENTS

We thank Noam Bernstein, Joseph L. Feldman, and Michael J. Mehl for helpful discussions. This work is supported by the U.S. Department of Energy.

[1] J. C. Slater and G. F. Koster, Phys. Rev. **94**, 1498 (1954).
[2] D. A. Papaconstantopoulos and M. J. Mehl, J. Phys.: Condens. Matter **15**, R413 (2003).
[3] D. A. Papaconstantopoulos, *Handbook of Electronic Structure of Elemental Solids* (Plenum, New York, 1986).
[4] M. J. Mehl and D. A. Papaconstantopoulos, Phys. Rev. B **54**, 4519 (1996).
[5] R. E. Cohen, M. J. Mehl, and D. A. Papaconstantopoulos, Phys. Rev. B **50**, 14694, (1994).
[6] F. Kirchhoff, M. J. Mehl, N. I. Papanicolaou, D. A. Papaconstantopoulos, and F. S. Khan, Phys. Rev. B **63**, 195101 (2001).
[7] S. W. Wei and M. Y. Chou, Phys. Rev. Lett. **69**, 2799 (1992).
[8] B. M. Klein and R. E. Cohen, Phys. Rev. B **45**, 12405, (1992).
[9] S. C. Miller and W. F. Love, *Tables of Irreducible Representations of Space Groups and Co-Representations of Magnetic Space Groups* (Pruett, Boulder, CO, 1967).
[10] H. T. Stokes and D. M. Hatch, *Isotropy Subgroups of the 230 Crystallographic Space Groups* (World Scientific, Singapore,

1988).
[11] A. P. Miller and B. N. Brockhouse, Phys. Rev. Lett. **20**, 798 (1968).
[12] M. J. Mehl, B. M. Klein, and D. A. Papaconstantopoulos, in *Intermetallic Compounds: Principles and Applications*, edited by J. H. Westbrook and R. L. Fleischer (Wiley, London, 1994), Vol. 1.
[13] D. K. Hsu and R. G. Leisure, Phys. Rev. B **20**, 1339 (1979).
[14] D. A. Papaconstantopoulos and D. J. Singh, in *NATO ASI Series*, edited by P. E. A. Turchi and A. Gonis (Plenum, New York, 1994), Vol. 319, pp. 439–442.
[15] A. C. Bailey, N. Waterhouse, and B. Yates, J. Phys. C **2**, 769 (1969).
[16] L. M. Peng, G. Ren, S. L. Dudarev, and M. J. Whelan, Acta Crystallogr. **52**, 456 (1996).
[17] C. V. Pandya, P. R. Vyas, T. C. Pandya, and N. Ranil, and V. B. Gohel, Physica B **307**, 138 (2001).
[18] F. E. Hoare and B. Yates, Proc. R. Soc. London, Ser. A **240**, 42 (1957).
[19] L. D. Landau and E. M. Lifshitz, *Statistical Physics (Part 1)* (Pergamon, Oxford, 1980).